Performance-based design of bridge piers in liquefiable sites with shallow foundation and limited ground improvement

G. Bouckovalas
Department of Geotechnical Engineering – National Technical University of Athens, Greece
I. Psycharis, C.J. Gantes
Department of Structural Engineering – National Technical University of Athens, Greece
A. Sextos, A. Kappos
Department of Civil Engineering – Aristotle University of Thessaloniki, Greece
G. Mylonakis
Department of Civil Engineering – University of Patras, Greece

ABSTRACT
The common design practice for the foundation of heavy structures, such as bridge piers, in liquefaction prone areas is to use piles in order to transfer the foundation loads to deeper non-liquefiable soil layers. In parallel, it is often required to improve the liquefiable soil layers between and around the piles so that bending moments and pile head deflections do not become excessive. Nevertheless, recent experimental and theoretical studies suggest that the existence of a natural or artificially created (i.e. by ground improvement) surface "crust" of non-liquefiable soil, may mitigate the consequences of liquefaction in the subsoil, so that the use of shallow foundations becomes also permissible. In view of the above, a four-year research project was undertaken, aiming at extending and rationalizing the above findings into a novel practically oriented methodology for the seismic design of low cost surface foundations on liquefiable soils covered by a non-liquefiable "crust" of improved ground. Apart from replacing the more expensive pile foundation, this new design concept has the additional advantage of drastically reducing the inertia forces acting on the superstructure, as the un-improved liquefiable soil layers (below the crust) will act as a natural seismic isolation system. This paper presents the milestones of the performed research, with emphasis on assumptions and results, as well as on references for further study. The anticipated benefits from the new design approach are evaluated by means of a pilot application for relatively heavy superstructure conditions, namely for three common bridge types with different construction material and structural system: a statically determinate RC bridge; a statically indeterminate RC bridge; and an arch steel bridge.

1 INTRODUCTION

1.1 State of the Art & Background

It is the international practice today to prohibit the use of shallow foundation for heavy structures in liquefiable sites. Hence, piles are exclusively used, to transfer the foundation loads to deeper, non-liquefiable soil layers [Fig. 1(a)]. In order to reduce bending moments and to control lateral pile deflections, it is also required to improve the liquefiable soil using drains, stone columns, vibrocompaction, etc. (e.g. Jackura and Abghari, 1994, Liu et al. 1997, Ganev et al. 1998, Hausler and Sitar 1999, Cubrinovski et al. 2001, Biesiadecki et al. 2004, Comboult et al. 2005, Pecker 2006, Shin et al. 2008).

Nevertheless, field observations from strong earthquakes (e.g. Adachi et al. 1992, Ishihara et al. 1993, Acacio et al. 2001, Coehlo et al. 2005) and a number of recent experimental and numerical studies (e.g., Farrel and Kutter 1993, Naesgard et al. 1997, Cascone and Bouckovalas 1998, Kawasaki et al. 1998, Bouckovalas et al. 2005, Elgamal et al. 2005, Bird et al. 2006, Bouckovalas and Dakoulas 2008, Dashti et al. 2008, Bouckovalas et al. 2011) have shown that shallow foundations may also meet performance criteria in liquefiable sites so that the aforementioned (heavy duty) conventional design philosophy may be changed in favor of an overall less expensive structure and foundation design. The basic prerequisite for the use of surface foundations is the existence of a "crust" of non-liquefiable soil (e.g. clay, dense sand and gravel, or partially saturated-dry soil), with sufficient thickness and shear strength, which will be able to carry the foundation loads during the critical period after the end of shaking while the deeper soil layers are still at a liquefied state. Similar results can be obtained with the creation of an artificial "crust" of non-liquefiable soil using one of the available methods for soil improvement against earthquake-induced liquefaction (vibrocompaction, gravel piles, deep soil mixing, etc.) [Figure 1(b)].

For instance, refer to the case of Dagupan City in Philippines, during the 1990 Luzon Earthquake, where many buildings suffered settlements of 0.50 m in average and more than half tilted more than 1°. At this site, the 2.0 to 8.0 m thick sandy liquefied layer is overlaid by a surface "crust" of sandy/clayey silt deposits, which contains more than 40% fines and are therefore not susceptible to liquefaction (Ishihara et al, 1993). Tokimatsu et al (1994) were among the first to observe that there was a tendency for increasing damage with decreasing thickness of the non-liquefiable "crust". Furthermore, Acacio et al (2001) plotted data points from

damaged and undamaged buildings (Figure 2), in a graph of Z_{liq}/D versus H/D, where D is the foundation's embedment depth, while H and Z_{liq} are the thicknesses of the surface "crust" and the underlying liquefied layer respectively. Thus, they came up with a boundary curve (blue line in Figure 2) between damaged and undamaged foundations, corresponding to "crust" thickness ratio H/D=2÷4, depending on the thickness of the liquefied soil layer.

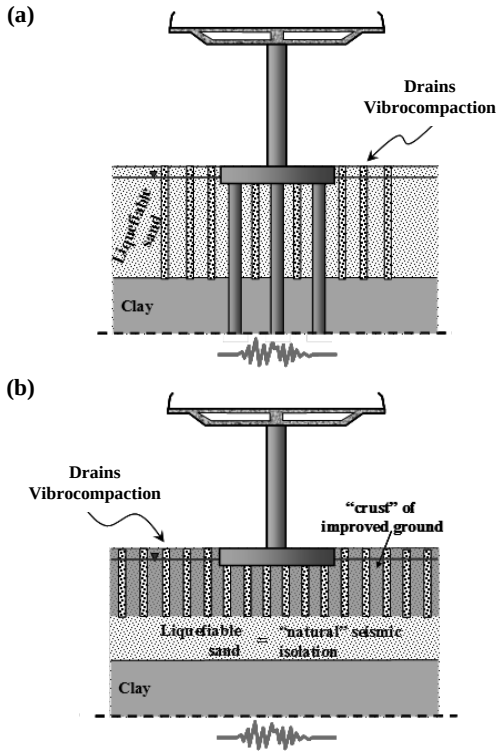

Figure 1. (a) Conventional and (b) novel foundation design

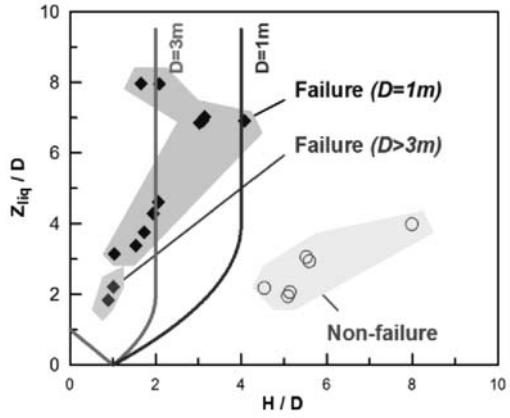

Figure 2. Effect of non-liquefiable soil crust on building damage (from Acacio et al. 2001)

1.2 Objectives and Milestones of Performed Research

The aim of the research reviewed herein was to extend and rationalize the above findings into a novel analytical (seismic code oriented) methodology for the seismic design of low cost surface foundations on liquefiable soils covered by a non-liquefiable "crust", as schematically presented in Figure 1(b). Emphasis is given to the case where the aforementioned "crust" is artificially constructed by partial (with depth and horizontal extent) ground improvement with gravel drain installation and/or vibrocompaction of the liquefiable soil.

It is noted that, apart from replacing the conventional method of pile foundation, this new design approach has the additional advantage of reducing the inertia forces acting on the superstructure, as the part of the subsoil which will be intentionally allowed to liquefy [see Figure 1(b)] will lose its shear resistance and will thus act as a "natural" seismic isolation system. However, it should be acknowledged that there are also some potentially detrimental effects that are related to the new design concept and need to be carefully considered. For instance, shallow foundations are admittedly more sensitive to differential settlements, which are likely to create additional actions to statically indeterminate superstructures. Furthermore, the creation of a natural seismic isolation system will not only reduce the peak seismic acceleration at the ground surface, but it will also move the frequency content of the seismic excitation to higher periods (lower frequencies), which may approach the fundamental vibration period of tall bridge piers and possibly lead to resonance amplification of the seismic loads. Such side effects will have to be explored in detail and minimized as they may act competitively to the anticipated benefits from the new design philosophy.

The key milestones of the performed research are listed below, and described briefly in the following sections with emphasis on assumptions and main findings. In parallel, reference is provided to relevant publications, which present each of the following topics in more detail.

(a) Analytical methodology for *shallow foundation design*, with special reference to the estimation of the degraded static bearing capacity at the end of the ground shaking, while the subsoil is still in a liquefied state, and the settlements accumulated during the seismic shaking.

(b) Analytical definition of the *elastic design response spectra* at the surface of liquefiable sites, to be used for the structural design, taking into account the intensely nonlinear, hysteretic response of the liquefied layers in the subsoil.

(c) Analytical definition of the equivalent distributed (Winkler type) *soil springs and dashpots,* which will be used to simulate soil-foundation-structure interaction effects for the dynamic response analysis of the superstructure.

(d) *Pilot application* of the new design philosophy for relatively heavy superstructure conditions, namely for three common bridge types with different construction material and structural system: a statically determinate RC bridge, a statically indeterminate RC bridge and an arch steel bridge.

(e) *Seismic Design Guidelines* which can be incorporated to seismic codes [e.g. Eurocode 2 (Part 2), Eurocode 8 (Parts 1& 2), Eurocode 7].

2 DESIGN SPECTRA FOR LIQUEFIABLE SITES

As mentioned previously, a main effect of liquefaction in the foundation soil is to reduce drastically the intensity of seismic motion at the surface of the liquefiable ground, relative to the outcropping seismic bedrock. This potentially beneficial effect may be definitely predicted by state-of-the art numerical analyses, as those performed to produce the database for the present study and will be briefly presented in later sections. Nevertheless, such methodologies are not appropriate for common applications, since they require expert knowledge and specialized input from advanced laboratory and field testing. Hence, one of the aims of this research was to develop simple numerical means (e.g. SHAKE-type, 1D wave propagation analyses) for the prediction of the elastic response spectra of liquefiable sites, which can be readily used in practice. This aim was achieved in the following two basic steps.

In the first step, a large number of 1D nonlinear numerical analyses of seismic ground response was performed parametrically with the finite difference code FLAC (Itasca 2011). The examined soil profile consisted of a non-liquefiable clay crust, underlain by a liquefiable sand layer of variable thickness followed by a non-liquefiable clay bed (Figure 3). The NTUA-SAND critical state plasticity constitutive model (Papadimitriou and Bouckovalas 2002; Andrianopoulos et al. 2010; Karamitros 2010) was employed for the liquefiable sand layer and the simpler Ramberg and Osgood (1943) nonlinear hysteretic model was selected for the non-liquefiable crust and the bed clay layers. The NTUA-SAND model was calibrated against monotonic and cyclic tests on saturated fine Nevada Sand presented by Arulmoli et al. (1992), while the Ramberg and Osgood model was calibrated against the experimental modulus reduction and damping curves of Vucetic and Dobry (1991) for low plasticity (PI = 30) clays. Tied-node conditions were applied at the lateral boundaries, which impose the same vertical and horizontal displacements to grid-points at the same elevation. An extra zone of the same size, but with elastic properties, was attached to the base of the soil column in order to simulate a compliant bedrock. The parametric study considered ten different sand layers, with five different thickness values H_L = 2 to 10 m (at 2 m increments) and two relative densities D_r = 40 and 60%. The selection of the seismic excitations was based on two criteria: (a) they were recorded at the surface of stiff soil - soft rock formations, similar to the ground category B of EC-8; and (b) their elastic response spectra resembled the corresponding spectra of EC-8 for strong seismic motions (M_w > 5.5). To examine the effect of shaking intensity, two different seismic excitation scenarios were considered: one with peak outcropping bedrock acceleration PGA = 0.30 g and the other with PGA = 0.15 g.

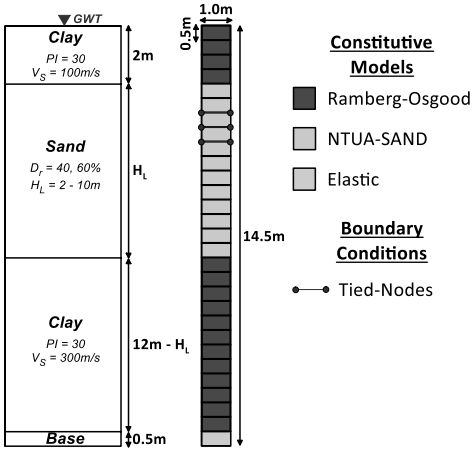

Figure 3. Soil profile, finite difference mesh and range of input parameters used in the parametric numerical simulation

In the second step, two alternative methodologies were conceptually developed based on previously published research, and quantitatively calibrated against the aforementioned numerical analyses:

(a) The *Spectral Interpolation* method, where the required elastic response spectra for a given factor of safety against liquefaction, FS_L, are computed by interpolation between the spectra for completely liquefied ground (FS_L < 0.30) and for non-liquefiable ground (FS_L > 1.20). The analyses for the non-liquefied and the liquefied sites are performed with common (e.g. equivalent linear) algorithms, while the in situ shear wave velocity is used for the non-liquefied soil and 10-20% of this value is used for the liquefied soil.

(b) The *Spectral Envelope* method, where the required elastic response spectra are computed as the upper envelope of the elastic response spectra for the pre- and the post-liquefaction segments of the seismic excitation. The pre- and the post-liquefaction analyses are performed with common equivalent linear algorithms, while the in situ shear wave velocity is used for the pre-liquefaction part of the seismic excitation and 10-20% of this value is used for the post-liquefaction part of it. The time of liquefaction onset at the ground surface is estimated as a function of the factor of safety against liquefaction FS_L.

Typical predictions with the above simplified methodologies are shown in Figures 4a & b, for two field case studies: the Superstition Hills (1987, M_w = 6.6) earthquake recorded at the Wildlife liquefaction array (WLA) in USA (Holzer et al. 1989) and the Kobe (1995, M_w = 6.9) earthquake recorded at the Port Island downhole array (PIDA) in Japan (Iwasaki and Tai 1996). In both cases, acceleration time-histories were recorded at the ground surface, as well as below the liquefied layer. The elastic response spectra of the former recordings are shown with thick continuous line, while those of the latter are shown with dotted line. It is observed that the simplified reproduce fairly well the basic features of the recorded motions. More specifically, for the WLA case study, where liquefaction occurred at the final stages of

strong shaking (average FS_L = 0.8), recorded and predicted ground motions remain rich at the low period range T = 0.3 - 0.8 s. On the contrary, for the PIDA case study, where liquefaction occurred early during shaking (average FS_L = 0.4), the predominant spectral amplitudes have shifted to the high period range, T = 1.0 - 2.2 s.

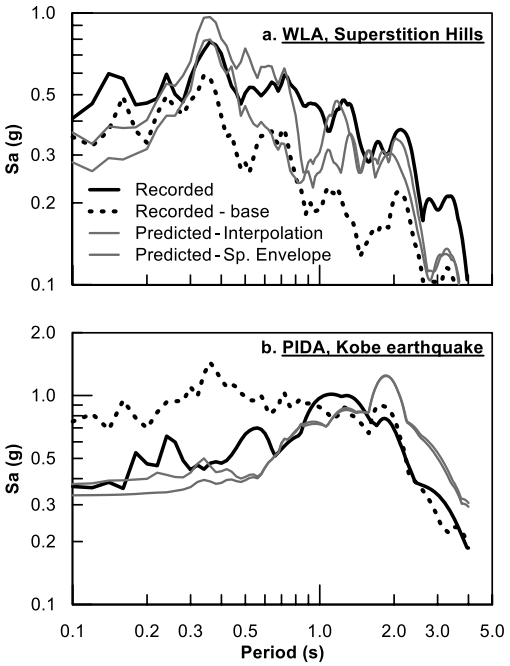

Figure 4. Evaluation of the *Interpolation* and the *Spectral Envelope* simplified methodologies for (a) WLA during the Superstition Hills earthquake and (b) PIDA during the Kobe earthquake.

Details on the aforementioned simplified design methods are given in Bouckovalas and Tsiapas (2015), Bouckovalas et al. (2016) and Tsiapas (2017). It is of practical interest to note that, regardless of the applied simplified method, elastic response spectra for liquefiable sites depend largely on the in situ factor of safety against liquefaction, FS_L, a site parameter that is routinely evaluated in practice. Furthermore, it was shown that the *Interpolation* method may be readily introduced to seismic codes, after adding one more site category for liquefied ground and establishing the corresponding design spectrum.

Finally, it is of practical interest to point that the results of the parametric numerical analyses performed for this research task have shown that predicted spectral accelerations for liquefied soil profiles are significantly less than those predicted ignoring liquefaction, at least for the low structural period range (e.g. T_{str} < 0.6 - 0.8 s). This effect, which is further discussed in connection with the pilot application of the proposed methodology that follows, may be interpreted as "natural seismic isolation" of the seismic actions applied to common structures, in the low period range. However, spectral accelerations may increase upon liquefaction for larger structural periods and this effect should be definitely accounted for in the design of tall and flexible structures (e.g. with T_{str} > 0.8 s).

3 SOIL SPRING AND DASHPOTS FOR FOOTINGS IN LIQUEFIABLE SITES

The aim of this research task was to provide analytical expressions for the frequency dependent parameters of the soil springs and dashpots, which are attached at the base of the superstructure (Figure 5a) in order to simulate the interaction of the foundation with the subsoil, both prior and after liquefaction. For non-liquefiable soil profiles, this method is well established (at least for homogeneous half-space conditions) and a number of different solutions are available for footings of various shapes and for profiles of various dynamic soil properties (e.g., Gazetas 1991, Vrettos 1999, Mylonakis et al 2006, Drosos and Mylonakis 2008). Nevertheless, such solutions are not applicable to liquefiable soil profiles, for two main reasons: (a) the existence of multi-layer soil profile (e.g. non-liquefiable crust – liquefiable layer – non-liquefiable base layer) with intense impedance contrasts between the layers, leading to entrapment of the seismic waves within the liquefied soil layer; and (b) the mostly unknown mechanisms of seismic wave propagation within liquefied soil layers, where the effective stresses and the wave propagation velocity may change even within each loading cycle.

To explore the above issues, a numerical study of the dynamic stiffness of a rigid surface footing resting on liquefiable soil under external harmonic loading was performed. The assumptions and the results of this research task are presented in detail by Karatzia et al. (2017) and briefly discussed in the following sections. In particular, the 3-layer soil profile shown in Figure 5b is considered, consisting of a surface non-liquefiable crust over a loose liquefiable sandy layer resting on a stiff base stratum. The numerical analyses covered a wide range of square footing sizes and excitation frequencies, ranging from 2 to 7 m and from 0 to 30 Hz, respectively. Thus, over 3×10^3 analyses were conducted in total.

The dynamic impedance of the footing is expressed by a static component, K^0_{ij}, and two dimensionless dynamic modifiers, k_{ij} and c_{ij}, corresponding to a storage stiffness (spring value) and a loss stiffness (damping value), related as:

$$S_{ij}(a_0) = K^0_{ij} [\, k_{ij}(a_0) + i\, a_0\, c_{ij}(a_0)] \qquad [1]$$

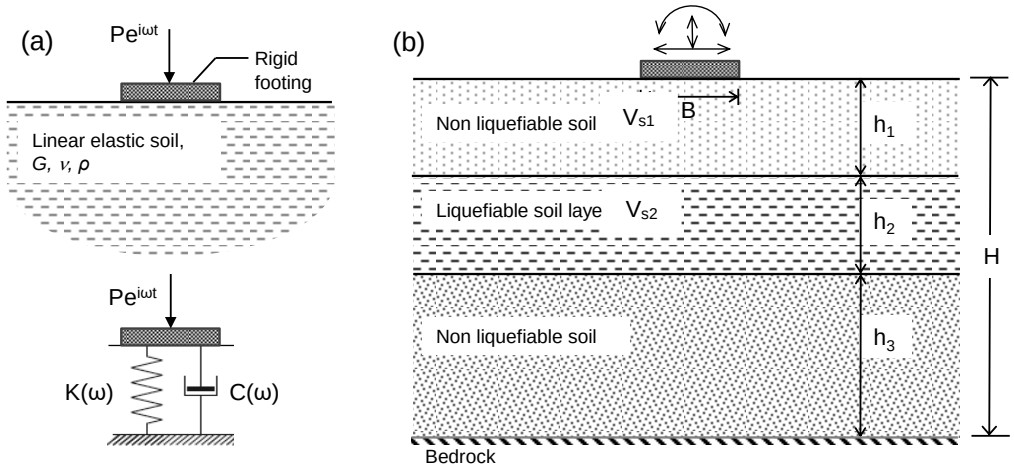

Figure 5. (a) Physical interpretation of dynamic stiffness, (b) Problem definition (from Karatzia et al. 2017)

where $a_0 = \omega B/V_s$ is a dimensionless frequency and B is the foundation width (Figure 5). Vertical, horizontal and rocking oscillations were considered, leading to three static stiffness components and six dynamic modifiers. The dynamic stiffness coefficients were evaluated by means of both 3D Finite Element analyses and simplified Cone models based on Strength-of-Materials theory, with the associated results found in fair agreement.

Table 1 presents typical results for the normalized static stiffness of square rigid footings for both pre-liquefaction (V_{s1}/V_{s2} = 0.67 and 1.67) and post-liquefaction (V_{s1}/V_{s2}=4 and 10) conditions, for the horizontal oscillation mode. It is first observed that the stiffness degradation of the liquefied soil stratum (i.e. the case of increased shear wave velocity ratio V_{s1}/V_{s2}) results in a decrease of the static stiffness coefficient, ranging from 14% to 55%. The highest decrease upon liquefaction is observed for a soft top layer (i.e. initial shear wave velocity ratio V_{s1}/V_{s2} = 0.67), as in the opposite case (i.e. of a stiff top layer) the overall rigidity of the subsoil remains high, even in presence of the liquefied underlying soil stratum. In addition, it becomes evident that the values of the post-liquefaction static stiffness coefficient increase as the crust thickness ratio h_1/B increases. This is reasonable if one considers that, for a thick top layer, the pressure bulb beneath the loaded area (about 1.5 B in diameter) does not extend to the soft underlying liquefied soil. Finally, it is observed that the increase in thickness of the liquefiable soil (h_2/B) seems to further reduce the static stiffness coefficient. This is because the stiff non-liquefiable base clayey layer is located in greater depth, providing extra rigidity to the foundation, thus, reducing the stiffening of the foundation response.

Results for dynamic impedance functions, for the typical case of horizontal oscillation of square footings on liquefiable three-layer soil profile, are depicted in normalized form in Figure 6. $\bar{K}_i$ and $\bar{C}_i$ refer to post-liquefied dynamic stiffness and damping, while K_i and C_i refer to pre-liquefied stiffness and damping values, respectively. Inspection of this figure reveals the existence of two regions, (I) and (II). *Region (I)*, defined for $\omega h_1/V_{s1}$<1.0, refers to common structures with footings having small to moderate width, B=1~3 m, (h_1 is comparable to B), profiles with soft soil crust, V_{s1}=100~150 m/s, and frequency range f =0~10 Hz. *Region (II),* defined for $\omega h_1/V_{s1}$ > 1.0, refers to large width footings, B > 4 m, profiles with soft to moderate soil crust, V_{s1}=100~250 m/s, and high frequency range f > 15 Hz. Observe that the dynamic stiffness is considerably reduced in *Region (I)*, while the corresponding dynamic damping ratio $\bar{C}_i/C_i$ increases well above unity. For *Region (II)*, the dynamic stiffness seems to amplify exhibiting sharp undulations, while $\bar{C}_i/C_i$ ratio tends to unity. It is noted that the same trends apply for the vertical and rocking oscillation modes as well, with the only difference being that the bound between these two regions is increased to $\omega h_1/V_{s1}$ = 2.

Table 1. Horizontal (normalized) static stiffness $K_{ij}/(G\times B)$ of square rigid footings on a 3-layer liquefiable soil profile (from Karatzia et al. 2017)

		V_{s1}/V_{s2}			
		Pre-liquefaction		*Post-liquefaction*	
h_1/B	**h_2/B**	**0.67**	**1.67**	**4**	**10**
0.5	**0.5**	3.08	2.26	1.67	1.31
	1	3.02	2.17	1.39	1.18
	2	2.95	2.06	1.27	1.08
1.0	**0.5**	2.80	2.39	1.74	1.77
	1	2.75	2.32	1.66	1.64
	2	2.71	2.27	1.58	1.53
2.0	**0.5**	2.61	2.44	1.85	2.10
	1	2.60	2.42	1.82	2.02
	2	2.54	2.37	1.79	1.92

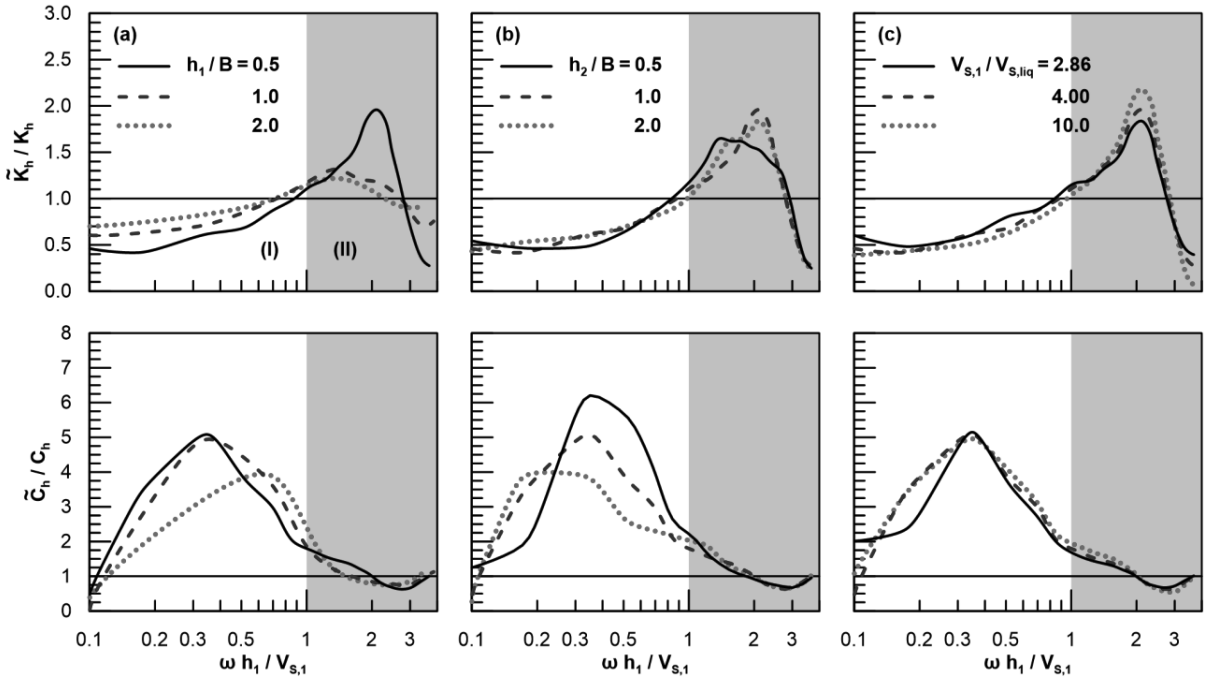

Figure 6. Post-liquefied horizontal dynamic impedance coefficients of square footing normalized with the corresponding pre-liquefied impedance coefficients. Effect of: (a) thickness of surface crust, (b) thickness of liquefiable soil layer, (c) shear wave velocity ratio. h_1/B = 0.5, h_2/B = 1, V_{s1}/V_{s2} = 2/3

4 ANALYTICAL METHODOLOGY FOR SHALLOW FOUNDATION DESIGN IN LIQUEFIABLE SITES

The numerical methodology used for the 1D seismic response analyses of liquefiable sites (Section 2) was extended for the 2D and 3D analyses of footings resting on liquefiable soil layers covered with a non-liquefiable crust. Following verification against relevant centrifuge experiments (Dimitriadi et al. 2015), more than 150 parametric analyses were performed and the results were statistically analyzed in order to provide analytical relationships for the following performance based design parameters:

(a) The *degraded factor of safety*, FS_{deg}, against static bearing capacity of the footing, at the end of shaking, while the soil is still at a liquefied state. This problem was initially approached with the help of existing static analytical solutions for 2-layered cohesionless soil profiles, where a relatively high strength crust covers a lower strength deep soil layer (Meyerhoff & Hanna 1978). In the sequel, the analytical solutions were calibrated against the results of the parametric numerical analyses.

(b) The *seismic settlements* which accumulate during shaking. In the absence of a similar analytical framework for the computation of seismic settlements, the numerical predictions were first analyzed for the effect of each individual problem (excitation, soil, foundation) parameter and, consequently, were composed into design oriented analytical relationships and charts using a multi-variable regression analysis.

Figure 7 shows the generic numerical model that was used for the parametric analysis of the footing response, for the 2D case of strip foundations on a crust of infinite lateral extent. The foundation is considered rigid, while it is assumed that the non-liquefiable crust has been artificially created by vibrocompaction and drain installation, so that excess pore pressures do not exceed 20-40% of the vertical effective geostatic stress. The numerical analyses were performed in three successive stages: (a) initial geostatic stresses were generated and the foundation load under static conditions was incrementally applied up to the desired contact pressure q; (b) a fully coupled effective stress dynamic analysis with parallel water flow was executed, subjecting the soil-foundation system into a harmonic seismic base excitation; (c) upon the end of shaking, and while the soil was still at a liquefied state, the contact pressure of the foundation was gradually increased until bearing capacity failure.

Figure 8 shows the composite failure mechanism adopted for the analytical computation of the degraded (end of shaking) bearing capacity, i.e. punching of the foundation through the improved top layer, followed by a generalized wedge-type failure within the liquefiable sand layer. A basic deviation of the conventional Meyerhoff and Hanna (1978) static failure mechanism was necessary in order to account for the dissipation of earthquake-induced excess pore pressures, from the liquefiable sand towards the much more permeable improved top layer, which results in the creation of a transition zone of partially liquefiable sand.

Numerically computed dynamic settlements, reduced for the effects of the seismic excitation (a_{max}, T_{exc} and N) and site (T_{soil}) characteristics, are related in Figure 9 to

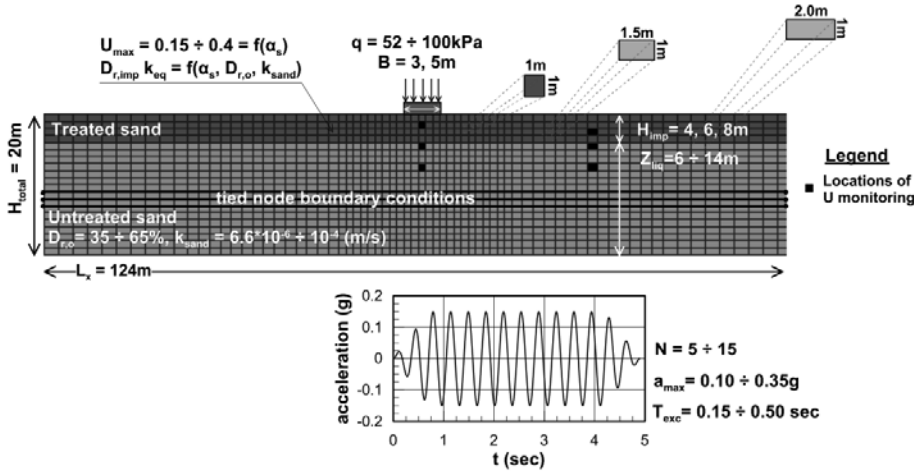

Figure 7. 2D Numerical model and input parameters used to analyze the response of strip foundation on improved soil crust with “infinite” lateral extend (from Dimitriadi et al. 2017a)

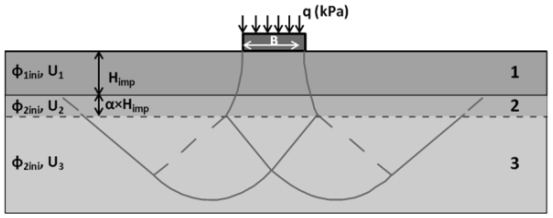

Figure 8. Failure mechanism of shallow foundation: (1) improved zone; (2) transition zone of partially liquefied ground; (3) liquefied ground (from Dimitriadi and Bouckovalas 2015)

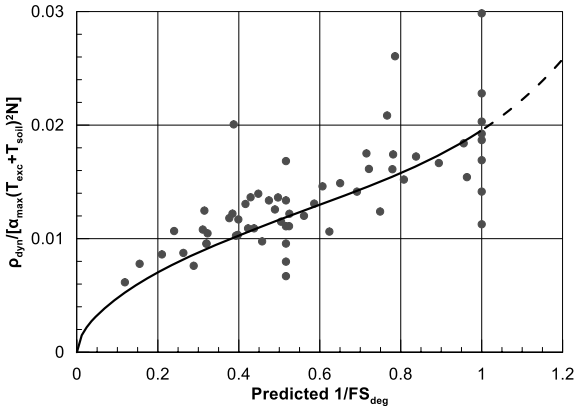

Figure 9. Variation of seismic settlement with the (inverse) degraded factor of safety - Strip foundations on improved soil crust with “infinite” lateral extend (from Dimitriadi et al. 2017a)

the inverse degraded factor of safety 1/FS_{deg} for the 2D case of strip foundations on an improved crust with "infinite" lateral extent. Observe that the rate of dynamic settlement accumulation tends to increase for degraded factors of safety FS_{deg} less than about 1.25 (i.e. 1/FS_{deg} > 0.80).

Figure 10 shows design charts that may be used to assess the effect of reduced ground improvement dimensions on settlements and degraded factors of safety, for the 2D case of strip foundations. To enhance the practical value of the charts, they are drawn in terms of a direct cost indicator, namely the volume of ground improvement $V_{imp}=B_{imp}\cdot H_{imp}$ per unit length of the strip foundation, for different values of the normalized thickness of the treated zone (H_{imp}/B). It is first observed that the rate of change in foundation settlements and degraded factors of safety is high for small values of the improved ground volume (i.e. for limited ground improvement) but it is drastically reduced after a certain point, indicating that the benefit in foundation response for further increase of the ground improvement dimensions becomes marginal.

The dashed lines in Figure 10 connect the points on the different design curves, beyond which the rate of foundation performance improvement, i.e. the $\rho_{dyn}/\rho_{dyn}^{inf}$ decrease and the FS_{deg}/FS_{deg}^{inf} increase, become lower than 5%. Thus, a second observation of interest is that, based on the particular criterion for the optimum cost wise ground improvement dimensions, seismic settlements reduction appears to be the controlling parameter for ground improvement design. This is because the optimum cost-over-benefit ground improvement for settlement reduction is obtained for V_{imp}/B^2 ≈ 1.0 to 7.0, and H_{imp}/B=0.5 to 2.0 respectively, as compared to the practically unique (independent from H_{imp}/B) value of V_{imp}/B^2 ≈ 1.0 required for the optimum cost-over-benefit improvement dimensions for degraded factor of safety increase.

The detailed development of the proposed methodology for performance based design of strip foundations, with “infinite” as well as limited dimensions of the improved crust, is presented in paper format by Dimitriadi & Bouckovalas (2015) and Dimitriadi et al (2015, 2017a and 2017b). The recently completed

extension to the general 3D case of rectangular footings and the resulting relationships are briefly outlined in the Appendix. Software (in Excel environment) for application of the proposed design methodology in practice is also available in web site http://www.georgebouckovalas.com (software section).

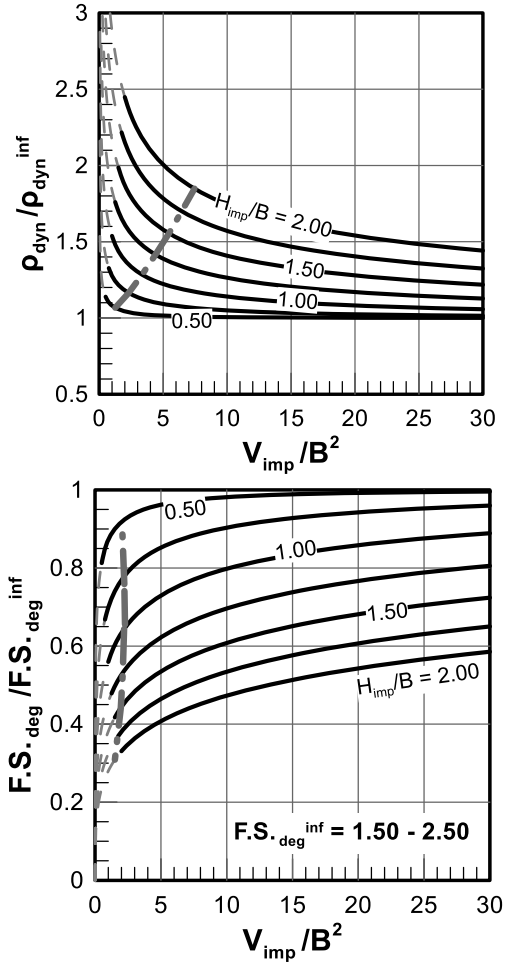

Figure 10. Correction factors for the effect of ground improvement dimensions on seismic settlement (ρ_{dyn}) and degraded static factor of safety (FS_{deg}) of strip foundations (from Dimitriadi et al., 2017b).

5 PILOT APPLICATION TO BRIDGE PIER DESIGN

To demonstrate the applicability and prove the feasibility of the novel natural soil isolation concept, three different bridge configurations were examined (Figure 11):

(a) The first bridge (Psycharis and Psilla, 2015) is a statically determinate, two-span (2×42 m) river crossing, concrete bridge. The deck is 11.25 m wide, plus 1.25 m wide pavements at each side, composed of 2×7 precast, 40.50m long pre-stressed concrete beams topped with a 0.25m thick cast in-situ slab. The concrete beams are resting upon the abutments and the mid-pier via elastomeric anchored bearings. The pier is a wall-type column of 1.50 m × 8.35 m cross section and 10.00 m free height.

(b) The second bridge studied (Sextos et al., 2015) is a statically indeterminate three-span concrete overpass of 99.00 m total length. The two outer spans have a length of 27.00 m each, while the middle span is 45.00 m long. The slope of the structure along the bridge longitudinal axis is constant, equal to 7% ascending towards the west abutment. The deck consists of a 10.00 m wide, pre-stressed concrete box girder section, while the two piers have a solid circular section of diameter equal to 2.00 m and free height of 7.95 m (left) and 9.35 m (right). Both piers are monolithically connected to the deck.

(c) The third bridge (Gantes and Vassilopoulou, 2015) is a two span, simply supported steel arch road bridge with 87.60m total length and 15.00 total deck width Each span is formed by two arches of 10.00m rise, interconnected with a bracing system. Two main beams are suspended from the corresponding arch with hangers and they are connected with seventeen transverse beams (HEB900). The composite deck, having a total thickness of 0.35m, is formed by trapezoidal profiles and a concrete slab, connected with the transverse and main beams through steel shear connectors. The connection of the deck to the pier and the abutments is realized with anchored elastomeric bearings. The pier consists of three 8m tall circular reinforced concrete columns, 1.50m in diameter, which are connected at the top with a 17.00m long and 2m high concrete beam.

All bridges were deliberately selected with approximately equal overall and span lengths, while the normalized vertical load at the piers were also kept at the same level. The foundation soil for the piers corresponds to an actual crossing of Egnatia Odos with Strymonas river in Northern Greece and consists mainly of 23.00 m thick liquefiable alluvia (Figure 12). The abutments were assumed similar, with a backwall height of 2.00 m, and supported on firm (non-liquefiable) soil formations. Furthermore, in all above bridges, the conventional design of the pier foundation consisted of a pile cap, resting at about 3.00 m depth from the free ground surface, and a group of cylindrical concrete piles. In the first bridge, the pile group includes 4×3 piles with diameter D = 1.00 m and length L = 25.00 m, while in the second bridge the foundation of each pier is made of a set of 3×3 piles with D = 1.00 m and L = 15.00 m and in the third bridge a group of 4×2 piles with D = 1.20 m and L = 25.00 m is used. To avoid over-stressing of the piles during seismic shaking, the soil between the piles is improved against liquefaction (i.e. by vibro-compaction and gravel pile installation) over the entire thickness of the liquefiable layers.

Two seismic scenarios were assumed for the design of the bridges: Scenario 1 with return period T_r = 225 yrs, corresponding to the *Operation Basis Earthquake*; and scenario 2 with return period T_r = 1000 yrs, corresponding to the *Maximum Design Earthquake* for bridges of high importance. Based on the seismicity of the Strymonas river crossing, which was chosen as representative for this pilot study, the magnitude of the seismic motion and

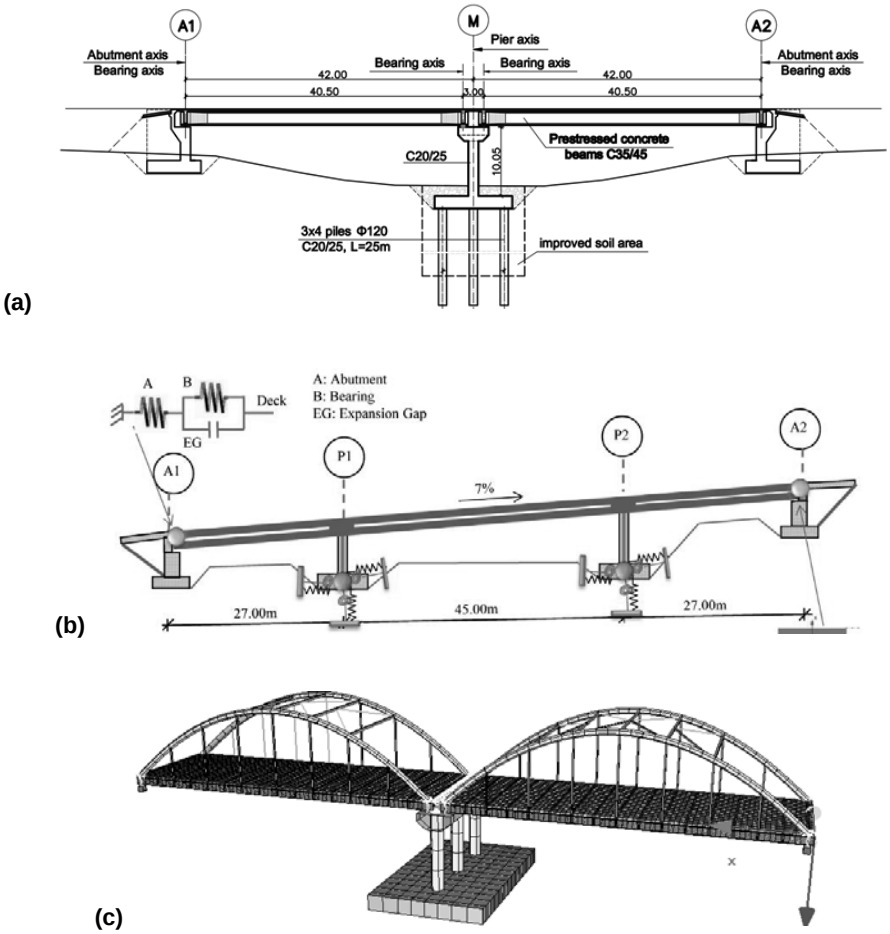

Figure 11. Bridge configurations considered in the pilot study: (a) statically determinate RC bridge; (b) statically indeterminate RC bridge; and (c) arched steel bridge.

the peak ground acceleration at the outcropping bedrock were: M_w = 6.2 and PGA_b = 0.22 g for the T_r = 225 yrs event; and M_w = 7.0 and PGA_b = 0.32 g for the T_r = 1000 yrs event. Liquefaction analysis of the soil profile shown in Figure 12 showed that increased liquefaction hazard would be provoked by the T_r = 1000 yrs event (average FS_L = 0.50) as opposed to the T_r = 225 yrs event which does not provoke liquefaction (average FS_L = 1.30) at the bridge site. For each seismic scenario, a suite of seven ground motion recordings was chosen, so that the average elastic response spectrum for 5% damping fits the design spectrum for soil category B of EC8, normalized to the above PGA_b values, and for structural periods in the range from 0.1 to 1.2 s (Figure 13).

In the sequel, both seismic scenarios were analyzed to obtain the design spectra at the free ground surface of the pier site, for the natural as well as for the improved (against liquefaction) ground conditions. The resulting design spectra are shown in Figure 14 for three different soil and seismic excitation combinations: (a) T_r = 1000 yrs and improved ground; (b) T_r = 225 yrs and natural soil conditions without liquefaction; and (c) T_r = 1000 yrs and natural soil conditions with liquefaction. The design spectra for the first two combinations (i.e without liquefaction in the foundation soil) were obtained with common equivalent-linear site response analyses, while the design spectra for the last combination (i.e. with liquefaction) were obtained with the numerical methodology outlined in Section 2.

It is further noted that the first spectrum was used for the analysis of the conventional pier design (Figure 1a), whereas both remaining spectra were employed for the analysis of the novel pier design (Figure 1b), as it was not a-priori known which one was the most critical. To this end, it is interesting to observe in Figure 14 that, for natural soil conditions, spectral accelerations for the strong seismic excitation (scenario 1) are 15 to 55% less than those for the weak seismic excitation (scenario 2), in the period range from 0.5 s to 1.0 s where the bridge piers operate. This difference is explained given that the weak excitation scenario does not lead to liquefaction of the subsoil and, consequently, it amplifies the seismic motion, contrary to the strong excitation scenario which leads to liquefaction of the subsoil that de-amplifies the seismic motion. In other words, it is verified that, allowing liquefaction in the subsoil may protect the superstructure

from extreme seismic events by triggering a "*natural seismic isolation*" system.

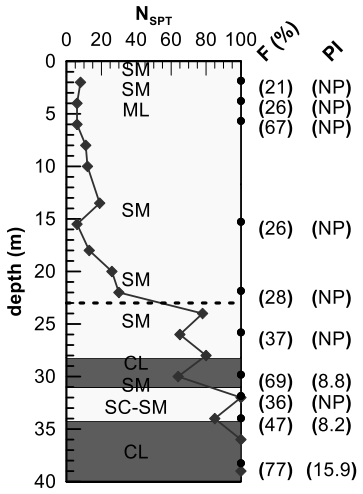

Figure 12. Soil profile for bridge pier foundation (the dotted line shows the maximum liquefaction depth)

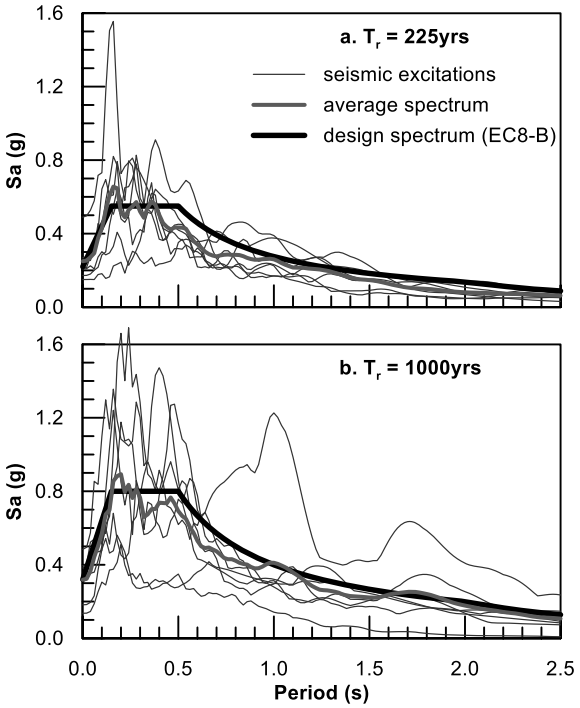

Figure 13. Elastic response spectra for the considered seismic excitations with T_r = 225 yrs and T_r = 1000 yrs return periods

A key issue for the novel foundation design of the bridge pier, i.e. with a spread footing instead of piles (Figure 1b), was to decide the dimensions of the improved soil area below the footing so that: (a) settlements during strong earthquake shaking and liquefaction (ρ_{sei}) remain below acceptable limits (ρ_{all}), and (b) the degraded static factor of safety FS_{deg} at the end of shaking is higher than 1.00. In the examined case studies, the afore-mentioned foundation performance indicators (ρ_{sei} and FS_{deg}) were evaluated with the methodology described in Section 4 and the Appendix. The allowable foundation movements (settlements and rotations) were established in accordance with the afforded damage and serviceability criteria (e.g. driving discomfort, repairable damage, non-repairable damage). It should be noted that liquefaction-induced displacements (in the form of settlements and rotations, see Figure 15) gradually accumulate during the seismic event. Therefore, these displacements should be considered as permanent actions, which may produce permanent additional stress and deformations to the structural components of the superstructure (piers, deck, bearings, etc.). It should be also pointed that these settlements are combined to "parasitic" footing rotations, along and transverse to the bridge deck, which have been approximately computed according to Yasuda et al. (2001) and Yasuda (2014) as ϕ(deg) = 0.05ρ (cm).

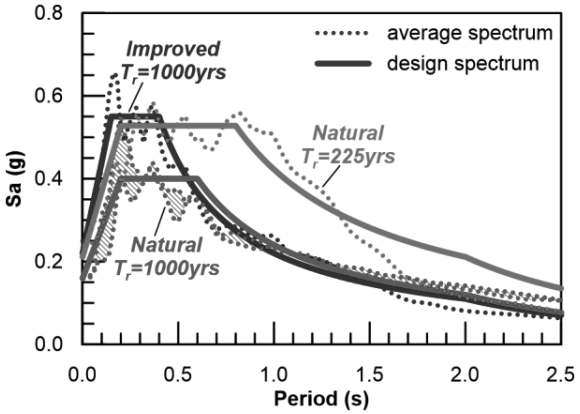

Figure 14. Design spectra for improved foundation soil (T_r = 1000 yrs) and for natural soil conditions (T_r = 225 yrs & T_r = 1000 yrs) at the pier site, adjusted to the corresponding calculated average response spectra

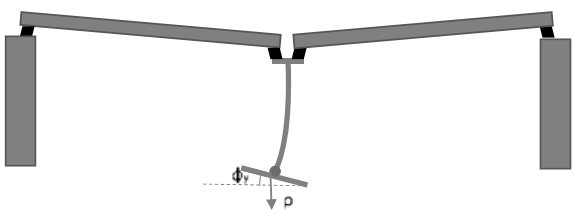

Figure 15. Pier yielding due to liquefaction-induced settlement and rotations at its footing

The steps to be followed to define the tolerable settlement, ρ_{all}, of a bridge founded over liquefaction susceptible soils, are:

(a) A preliminary, conventional, design of the bridge against static and seismic actions is carried out, in order to define the required dimensions and reinforcement of the various structural members.

(b) The yield bending moment, $MR_{d,y}$, of the critical sections of the piers (bottom and top) are calculated. To this end, the corresponding bending moment versus curvature plots are drawn (for both the maximum and the minimum axial load of the pier). Since the results are to be used for design purposes, design values should be used for the material properties.

(c) A nonlinear static (pushover) analysis under the persistent combinations of loads (as described in Eurocode 0) and step-wise gradually increasing settlements and rotations Δ at the base of the pier is performed, where $\Delta = \rho + \phi_y + 0.3\phi_x$ or $\Delta = \rho + \phi_x + 0.3\phi_y$.

The allowable settlement, ρ_{all}, is then defined as the critical settlement producing the predefined allowable rotational ductility at the critical section of the most unfavorable pier, divided by a safety factor of 1.15 according to Eurocode 0 for permanent imposed soil movements. Applying this procedure to the examined case studies it was found that the allowable footing settlements, due to static and seismic loading, varied as follows: ρ_{all} = 20 to 24 cm for the statically determinate RC and steel bridges and ρ_{all} = 13 cm for the statically indeterminate RC bridge.

Table 2 summarizes the characteristics of the footings, as well as the dimensions and performance (during the 1000 yrs strong shaking) of the applied ground improvement for the three typical bridges examined in the project. The first issue to observe is that performance requirements may be satisfied by a relatively limited ground improvement with thickness equal to $H_{imp} \approx (0.33 \div 0.38)B$ (B is the footing width), over an area $A_{imp} \approx (1.4 \div 1.5)A_{foot}$ ($A_{foot} = B \times L$ is the plan area of the footing). Moreover, seismic footing settlements (8.8 ÷ 13.8 cm) are sufficiently lower than the allowable ones for initiating damage to the superstructure (ρ_{sei} = 13 ÷ 24 cm). Taking further into account that the post-shaking static factors of safety (FS_{deg} = 1.50 ÷ 3.90) are clearly higher than 1.0, it is realized that the bridge maintains considerable strength even after the strong seismic shaking and the development of permanent settlements and rotations.

Table 2. Comparative presentation of ground improvement characteristics & performance

BRIDGE	RC ISO-static	RC HYPER-static	STEEL arch	RANGE
Footing				
$B \times L$ (m)	8.0x15.0	9.0x10.5	6.7x17.7	
L/B	1.9	1.2	2.6	1.2 ÷ 2.6
q_0 (kPa)	250	140	180	180 ÷ 250
Improvement				
A_{impl}/A_{foot}	1.4	1.5	1.4	1.4 ÷ 1.5
H_{impl}/B	0.38	0.33	0.37	0.33 ÷ 0.38
Performance				
FS_{deg}	1.80	3.90	1.50	1.50 ÷ 3.90
ρ_{dyn} (cm)	11.0	8.8	13.8	8.8 ÷ 13.8
ϕ (rad)	9.6 ‰	7.8 ‰	12.0 ‰	7.8 ÷ 12.0 ‰

Table 3 provides a techno-economical comparison between the conventional and the novel design, separately for each bridge type. It is observed that, for all bridge types, the novel design for the weak seismic motion (T_r = 225 yrs) and no liquefaction in the subsoil is more critical than the novel design for the strong seismic motion (T_r = 1000 yrs) and liquefaction in the subsoil, despite that permanent footing settlements in the latter case are much larger. This finding verifies that the "natural seismic isolation" provided by the novel bridge design protects the superstructure during extreme seismic events, which may even exceed the critical design excitation. The second interesting observation is that the benefits of the novel design are more pronounced for the iso-static RC and the steel bridges than for the hyper-static RC bridge. Namely:

(a) For the iso-static (statically determined) bridges maximum design bending moments and shear forces are reduced by 9÷15% and 27÷31% respectively, while the foundation cost is reduced by 63÷67% and the total cost (per span) is reduced by 17÷20%.

(b) For the hyper-static (statically indetermined) bridge, the corresponding reductions were 9.1%, 6.5%, 43.3% and 7.2%.

The price paid for the above benefits of the novel design is that permanent foundation settlements after the critical design ground motion (T_r = 1000 yrs) are much larger than those of the conventional design (i.e. 10.8 ÷ 16.0 cm as compared to 1.5 ÷ 2.0 cm). This finding implies that the over-stressed sections of the bridge might need to be enhanced/retrofitted after a strong seismic event, so that their capacity to sustain less intense after-shocks and future seismic motions, which may not cause liquefaction to the subsoil, will not be degraded.

Table 3. Technical and cost comparison of novel and conventional bridge design

(a) iso-static R.C. bridge	Conventional Design	Novel Design	
	1000yrs	225yrs	1000yrs
$M_{max,base}$ (MNm)	25.2	21.6 (-15%)	13.1 (-48%)
$Q_{max,base}$ (MN)	3.3	2.6 (-31%)	1.6 (-53%)
ρ_{total} (cm)	2.0	2.5	9.3
Foundation Cost (k€)	218	73 (-67%)	-
Total Cost*/span (k€)	870*	720 (-17%)*	-

(b) hyper-static R.C. bridge	Conventional Design	Novel Design	
	1000yrs	225yrs	1000yrs
$M_{max,base}$ (MNm)	28.7	26.1 (-9.1%)	24.6 (-14.3%)
$Q_{max,base}$ (MN)	6.2	5.8 (-6.5%)	5.3 (-14.5%)
ρ_{total} (cm)	1.5	2.0	7.7
Foundation Cost (k€)	90	51 (-43%)	-
Total Cost*/span (k€)	540*	501 (-7%)*	-

(c) Steel arch bridge	Conventional Design	Novel Design	
	1000yrs	225yrs	1000yrs
$M_{max,base}$ (MNm)	6.6	6.0 (-9%)	4.3 (-48%)
$Q_{max,base}$ (MN)	1.1	0.8 (-27%)	0.6 (-55%)
ρ_{total} (cm)	1.7	2.2	10.2
Foundation Cost (k€)	212	77.5 (-63%)	-
Total Cost*/span (k€)	1092*	871 (-20%)*	-

** Total costs were computed approximately for unit price 1500€/m² of deck*

6 STEP-BY-STEP APPLICATION OF DESIGN METHODOLOGY

The steps to be followed in order to apply the proposed design methodology in practice are described below:

(a) The liquefaction potential for the site of interest is evaluated based on existing geotechnical investigations for the following two seismic loading scenarios: a weak seismic motion (e.g. Operation Basis Earthquake with return period T_{ret} = 225 yrs) and a strong seismic motion (e.g. Design Maximum Earthquake with return period T_{ret} = 1000 yrs).

(b) The elastic design spectra at the ground surface are defined for the previous two seismic scenarios. Conventional procedures are used when the factor of safety against liquefaction exceeds about 1.20, while the procedures developed for liquefiable sites in the present project (section 2) are otherwise used.

(c) A preliminary design of the bridge with shallow foundation is carried out following the typical design procedure for bridges in order to determine the minimum dimensions of the footing and the structural members. At this stage, the support conditions of the pier, i.e. the characteristics of the springs and the dashpots at the base of the pier, may be assessed for the initial conditions without liquefaction.

(d) According to the results of step (c), the maximum allowable foundation movements, ρ_{all}, are calculated, taking also into account appropriate serviceability criteria. To this end, the diagram of the moments at the base of the pier (where the first plastic hinge is formed) against imposed settlements is produced and the procedure presented in Section 5 is followed.

(e) In case of liquefaction (i.e. in step a), the final dimensions of the footing, along with the dimensions of the improved crust are defined, so that the following two performance criteria are satisfied:

- The post-shaking static safety factor FS_{deg}, immediately after the strong seismic event should be larger than 1.10 to 1.20.
- The permanent total (static and seismic) settlements ρ following the strong seismic event should be lower than the maximum allowable foundation movements ρ_{all} which were established in the previous step (d).

For this purpose, the foundation design methodology described in Section 3 is applied iteratively (e.g. via spreadsheet programmed calculations) for various dimensions of the improved soil crust, until the minimum volume of ground improvement is achieved.

(f) Taking into account the dimensions of the footing, the structural and the excitation frequencies, as well as the dimensions of the improved soil crust, the static and

dynamic characteristics of the (Winkler) soil springs and dashpots are defined, as described in Section 4.

(g) Considering the design spectra, the dimensions of the footing and the characteristics of the soil springs defined in the previous steps, the bridge is now re-designed against seismic actions, for the following two conditions:

- No liquefaction state corresponding to the weak motion: The bridge should perform practically elastically ($q \leq 1.5$). This check corresponds to “Immediate Occupancy” performance level.
- Liquefaction state corresponding to the strong motion: The bridge should tolerate loads and displacements imposed during and immediately after the seismic motion. The asynchronous motion of abutment and pier due to different foundation conditions should be considered. This check corresponds to “Life Safety” performance level.

According to the results of the calculations, the final dimensions and reinforcement of the various members of the bridge are defined.

(h) In case that previous step (g) leads to different reinforcement ratio compared to what was computed during the preliminary design of the bridge in step (c), corresponding to a different resistance moment of the pier and different maximum allowable foundation settlements, ρ_{all}, steps (d) to (g) shall be repeated until convergence is achieved. Note that, in the pilot applications examined during the project, convergence was achieved after one such iteration.

7 CONCLUDING REMARKS

This paper presents an overview of a four-year joint research project aimed to examine the feasibility of using shallow foundations in liquefiable sites, combined with partial (with depth) improvement of the foundation soil. In the interest of space, the presentation focused on the objectives, assumptions and main findings of this research effort. Particular research topics have already been published in journals and conference proceedings, which are referred herein so that the interested reader has access to more information. The essence of the new foundation concept is:

(a) To verify the seismic response of the structure for the more frequent and relatively weak Operation Based Earthquake (OBE), instead of the less frequent and stronger Design Probable Earthquake (DPE), assuming that the former does not cause liquefaction in the foundation soil, being thus more critical than the latter.

(b) To verify the structural integrity of the super-structure against the differential settlements and footing rotations expected to develop due to liquefaction of the un-improved foundation soil during the Design Maximum Earthquake (DME).

The main finding of this study is that the proposed novel design concept is indeed feasible for relatively flexible structures, such as the isostatic bridges examined in the pilot application, leading to accountable savings in the foundation cost without compromising the performance of the entire structure. Further benefits, not explicitly accounted for in this study, may result from the reduced seismic loads acting on the superstructure due to the "soft" response of the liquefiable soil below the improved zone, which acts as a means of "natural seismic isolation" for commonly anticipated earthquake excitations.

Taking into account that our research was mainly based on parametric numerical analyses, without any intention to underestimate the efforts made to ensure the accuracy of the results, it is acknowledged that this is only the first step towards a widely accepted new design methodology that could be included in future seismic codes. The next step is the experimental verification and calibration of the proposed methodology through model and field case studies. In addition, there is a number of additional design issues which deserve attention.

For instance, foundation settlements during seismic loading and liquefaction are also accompanied by parasitic rotation, attributed to non-predictable accidental factors, such as loading eccentricities, geometry imperfections or laterally non-uniform soil conditions. In the present study it was approximately assumed that foundation rotation ϕ (deg) accounts for about 5% of the average settlement ρ (cm), as proposed by Yasuda, based on a relatively limited set of field observations for light buildings. However, the pilot application has shown that foundation rotation is quite important for the superstructure and deserves a more refined evaluation, especially in case of statically indeterminate structural systems.

A second important issue lies in the evaluation of the factor of safety against liquefaction (FS_L). This is because the currently available methods have been intentionally developed for conservative evaluation of the liquefaction susceptibility, so that proper action is taken in order to mitigate this detrimental effect. In that sense, it is quite probable that a site would not liquefy even though the computed FS_L is less than unity. It is realized that this approach is appropriate when designing liquefaction mitigation measures, but it may not work when applied to the proposed design methodology, where liquefaction in the untreated foundation soil is a prerequisite for achieving the intended "natural seismic isolation effect". In fact, no matter how counter-intuitive it may sound, the FS_L estimates in this case must be un-conservative enough so that liquefaction in the untreated soil is practically certain when the computed FS_L is less than 1.0.

8 ACKNOWLEDGEMENTS

This research has been co-financed by the European Union (European Social Fund - ESF) and Greek national funds through the Operational Program “Education and Lifelong Learning” of the National Strategic Reference Framework (NSRF)-Research Funding Program: THALES. Investing in knowledge society through the European Social Fund. Our gratitude is also due to the junior researchers who assisted the Authors in this joint project and their names appear in the independent papers and research reports referenced in the text.

9 REFERENCES

Acacio, A.A., Kobayashi, Y., Towhata, I., Bautista, R.T., Ishihara, K. 2001. Subsidence of building foundations resting upon liquefied subsoil: Case studies and assessment, *Soils and Foundations*, 41(6), 111-128.

Adachi, T., Iwai, S., Yasui, M. Sato, Y. 1992, Settlement and inclination of reinforced concrete buildings in Dagupan City due to liquefaction during 1990 Philippine Earthquake, *Proceedings of 10th World Conference on Earthquake. Engineering,* Balkema Rotterdam, 2, 147-152.

Andrianopoulos, K.I., Papadimitriou, A.G., Bouckovalas, G.D. 2010. Bounding surface plasticity model for the seismic liquefaction analysis of geostructures. *Soil Dynamics and Earthquake Engineering*, 30(10), 895–911.

Arurmoli, K., Muraleetharan, K K., Hossain M. M., Fruth L. S. 1992. *VELACS: verification of liquefaction analyses by centrifuge studies; Laboratory Testing Program – Soil Data Report*, Research Report, The Earth. Technology Corporation.

Biesiadecki, G.L., Dobry, R., Leventis, G.E. and Peck R.B. 2004. Rion – Antirion bridge foundations: a blend of design and construction innovation, *5th International. Conference on Case Histories in Geotechnical Engineering*, New York, NY, April 13-17.

Bird, J.F., Bommer, J.J., Crowley, H. and Pinho R. 2006. Modelling liquefaction-induced building damage in earthquake loss estimation, *Soil Dynamics and Earthquake Engineering*, 26(1), 15-30.

Bouckovalas, G.D., Valsamis, A.I., Andrianopoulos K.I. 2005. Pseudo static vs. performance based seismic bearing capacity of footings on liquefiable soil, *Proceedings of Geotechnical Earthquake Engineeiring Satellite Conference*, Osaka, Japan, September 10.

Bouckovalas, G.D. and Dakoulas, P. 2008. Liquefaction performance of shallow foundations in presence of a soil crust, I*nvited Lecture, Proceedings, Geotechnical Earthquake Engineering and Soil Dynamics IV*, Thessaloniki, June.

Bouckovalas, G.D., Madabhushi, S.P.G. et al. 2011. *Experimental Verification of Shallow Foundation Performance under Earthquake-induced Liquefaction*, Research Report, Foundation Engineering Laboratory (NTUA) in cooperation with The Schofield Center of Cambridge University.

Bouckovalas, G.D., and Tsiapas, Y.Z. 2015. Seismic Isolation Effects and Elastic Response Spectra of Liquefied Ground, *6th International Conference on Earthquake Geotechnical Engineering*, Christchurch, New Zealand, November 1-4.

Bouckovalas, G.D., Tsiapas, Y.Z., Zontanou, V.A., and Kalogeraki, C.G. 2016. Equivalent Linear Computation of Response Spectra for Liquefiable Sites: The Spectral Envelope Method. *Journal of Geotechnical and Geoenvironmental Engineering*. DOI: 10.1061/(ASCE)GT.1943-5606.0001625.

Cascone, E. and Bouckovalas, G. 1998. Seismic bearing capacity of footings on saturated sand with a clay cap", *11th European Conference in Earthquake Engineering*, Paris, September 6-11.

Coehlo, P., Haigh, S.K, Madabushi, S.P.G. 2005. Development, effects and mitigation of earthquake induced liquefaction: A comprehensive study based on dynamic centrifuge modeling, *Proceedings, 16th International Conference on SMGE*, Osaka, Japan

Combault, J., Pecker, A., Teyssandier, J.-P.., Tourtois, J.-M. 2005. Rion-Antorion bridge, Greece-concept, design and construction, *Structural Engineering International*, 12 (1).

Cubrinovski, M., Ishihara, K., Kijima, T. 2001. Effects of liquefaction on seismic response of a storage tank on pile foundations, *4th International. Conf. on Recent Advances in Geotechnical Earthquake Engineering and Soil Dynamics*, San Diego CA, March.

Dashti, S., Bray, J., Riemer, M. and Wilson, D. 2008. Centrifuge experimentation of building performance on liquefied ground, *Geotechnical Special Publication*, 181

Dimitriadi, V. and Bouckovalas, G. 2015. Analysis of Strip Foundation Performance on Liquefied Ground with Limited Ground Improvement, *XVI European Conference on Soil Mechanics and Geotechnical Engineering*, Edinburgh, UK, September 13-17.

Dimitriadi, V., Bouckovalas, G. and Chaloulos, Y. 2015. Numerical Analysis of Liquefaction affected Shallow Foundations Performance on Improved Ground, *XVI European Conference on Soil Mechanics and Geotechnical Engineering*, Edinburgh, UK, September 13-17.

Dimitriadi, V., Bouckovalas, G.D. and Papadimitriou, A.G. 2017a. Seismic performance of strip foundations on liquefiable soils with a permeable crust, *Soil Dynamics and Earthquake Engineering* (under review).

Dimitriadi, V., Bouckovalas, G.D. and Chaloulos, Y.K. 2017b. Effect of ground improvement dimensions on the seismic liquefaction performance of strip foundations, *Bulleting of Earthquake Engineering* (under review).

Drosos, S. and Mylonakis, G., 2008. Energy Solutions for Stiffness and Damping of Single Piles in Inhomogeneous Soil, *3rd Greek Conference on Earthquake Engineering*, November 5-7, Athens.

Elgamal, A., Lu, J. and Yang, Z. 2005. Liquefaction-induced settlement of shallow foundations and remediation: 3D numerical simulation, *Journal of Earthquake Engineering*, 9, 17-45.

European Committee for Standardization 2004. Eurocode 0, Eurocode 1, Eurocode 2, Eurocode 3, Eurocode 4, Eurocode 8, Brussels.

Farrell, T. M. and Kutter, B. L. 1993. *Experimental results of Model No 12, Verifications of Numerical Procedures for the Analysis of Soil Liquefaction Problems*, Balkema, Rotterdam, ISBN 90 5410 360 4.

Gazetas G. 1991. *Foundation vibrations, Foundation Engineering Handbook*, 2nd Ed., Springer, 15, 553-593.

Ganev, T., Yamazaki, F., Ishizaki, H. and Kitanazawa, M. 1998. Response analysis of the Higashi-Kobe bridge and surrounding soil in the 1995 Hyogoken-Nanbu earthquake, *Earthquake Engineering and Structural dynamics,* 27, 557-576.

Gantes, C. and Vassilopoulou, I. 2015. *Pilot seismic study of an arched steel bridge pier on liquefiable ground*. Research Report, NTUA (THALES MIS 380043).

Hausler, E. and Sitar, N. 1999. *Oriental Hotel on Merikan Wharf*, HKN028, Performance of soil improvement techniques in earthquakes: A research project of U.C. Berkeley.

Holzer, T.L., Youd, T.L., and Hanks, T.C. 1989. Dynamics of liquefaction during the 1987 Superstition Hills, California, earthquake. *Science*, 244(4900), 56–59.

Itasca 2006. *FLAC 3D – Fast Langrangian Analysis of Continua in 3 Dimensions*, Itasca Consulting Group Inc., Minenapolis,MN. (www.itascacg.com)

Itasca. 2011. *FLAC version 7.0*, Itasca Consulting Group Inc., Minenapolis, MN. (www.itascacg.com).

Ishihara, K., Acacio, A., Towhata, I. 1993. Liquefaction-induced Ground Damage in Dagupan in the July 16, 1990 Luzon Earthquake, *Soils and Foundations*, 33(1), 133-154.

Iwasaki, Y., and Tai, M. 1996. Strong motion records at Kobe Port Island, *Soils and Foundations*, (Special Issue), 29–40.

Jackura, K. and Abghari, A. 1994. *Mitigation of liquefaction hazards at three California bridge sites*, http://www.ceprode.org.sv/staticpages/pdf/eng/doc7479/doc7479-a.pdf

Karamitros, D.K. 2010. *Development of a Numerical Algorithm for the Dynamic Elastoplastic Analysis of Geotechnical Structures in Two and Three Dimensions,* PhD Thesis, Dept of Civil Engineering, NTUA, Athens.

Karatzia, X., Mylonakis, G., and Bouckovalas, G. 2017. 3D dynamic impedances of surface footings on liquefiable soil: Equivalent linear approach, *16th WCEE*, Santiago Chile, January 9-13.

Kawasaki, K., Sakai, T., Yasuda, S. and Satoh, M. 1998. Earthquake induced settlement of an isolated footing for power transmission tower, *Centrifuge* 98, 271-276.

Liu, H., Iai, S., Ichii, K., Morita, T. and Okashita, K. 1997. *Evaluation of deformation to the pneumatic caisson foundations of Kobe Ohashi bridge*, Report of Port and Harbour Research Inst., 36 (2), 19-39.

Meyerhof, G.G. and Hanna, A.M. 1978. Ultimate bearing capacity of foundations on layered soils under inclined load, *Canadian Geotechnical Journal*, 15, 565–572.

MCEER & FHA 2006. *Seismic Retrofiting Manual for Highway Structures: Part 1 – Bridges*, by I. G. Buckle (lead Author) et. al., FHWA-HRT-06-032.

Mylonakis, G., Nikolaou, S., and Gazetas, G. 2006. Footings under Dynamics Loads: Analysis and Design Issues with Emphasis on Bridge Foundations, *Soil Dynamics and Earthquake Engineering*, 26(9).

Mylonakis, G. 1995. *Contribution to Static and Seismic Analysis of Piles and Pile-Supported Bridge Piers*, Ph.D. Dissertation, Dept. of Civil Engineering, State University of New York at Buffalo.

Naesgaard, E., Byrne, P.M., and Ven Huizen, G., 1997. Behaviour of Light Structures Founded on Soil 'Crust' Over Liquefied Ground, *Geotechnical Special Publication*, 75: 422–433.

Papadimitriou, A.G. and Bouckovalas, G.D. 2002. Plasticity model for sand under small and large cyclic strains: A multiaxial formulation, *Soil Dynamics and Earthquake Engineering*, 22(3), 191–204.

Pecker, A. 2006. Enhanced seismic design of shallow foundations: example of the Rion-Antirion bridge, *4th Athenian Lecture on Geotechnical Engineering*.

Psycharis, I. and Psilla, N. 2015. *Pilot seismic study of a Statically Determinate bridge pier on liquefiable ground.* Research Report, NTUA (THALES MIS 380043).

Ramberg, W. and Osgood, W.R. 1943. *Description of stress-strain curve by three parameters.* Technical note 902, National Advisory Committee for Aeronautics.

Sextos A., Mylona E.-K., Kappos A. (2015). Pilot seismic study of a Statically In-determinate bridge pier on liquefiable ground. Research Report, NTUA (THALES MIS 380043).

Shin H., Arduino P., Kramer S.L. and Mackie K. 2008. Seismic response of a typical highway bridge in liquefiable soil, *Geotechnical Earthquake Engineering and Soil Dynamics IV*, Sacramento, California, US, May 18-22.

Tokimatsu, K., Kojimaa, H., Kuwayama, S., Abe, A., Midorikawa, S. 1994. Liquefaction-induced damage to buildings in 1990 Luzon Earthquake", *Journal of Geotechnical Engineering,* ASCE, 120(2), 290-307.

Tsiapas, Y.Z. 2017. *Seismic Response Analysis of Liquefiable Ground,* PhD Thesis, Dept of Civil Engineering, NTUA, Athens.

Vrettos, C. 1999. Vertical and rocking impedances for rigid rectangular foundations on soils with bounded non-homogeneity, *Earthquake Engineering and Structural Dynamics*, 28, 1525-1540.

Vucetic, M. and Dobry, R. 1991. Effect of soil plasticity on cyclic response. *Journal of Geotechnical Engineering*, 117(1), 89–107.

Yasuda S. 2014. Allowable Settlement and Inclination of Houses Defined After the 2011 Tohoku: Pacific Ocean Earthquake in Japan. *Earthquake Geotechnical, Geological and Earthquake Engineering*, Springer, 28, 141-157.

APPENDIX: Analytical computation of liquefaction-induced settlements and bearing capacity degradation of rectangular foundations on a locally improved liquefiable site

Table A.1: Input Data

	Footing		Excitation(1)
q:	net average contact pressure (kPa)	a_{max}:	Peak acceleration (m/s^2)
B:	Width (m)	N:	Number of cycles
L (>B):	length (m)	T_{exc}:	Period (s)
	Liquefiable Soil		Improved Soil
γ':	Buoyant unit weight (kN/m^3)(2)	B_{imp}:	width (m)
$\varphi_{2=}$ φ_3:	Friction angle (deg)	L_{imp}:	L+(B_{imp} - B)
Dr_o:	Relative Density (%)	U_{max}:	peak excess pore pressure ratio within the improved zone(3)
Z_{liq}:	Thickness below the improved zone (m)	k_{eq}:	equivalent uniform vertical permeability coefficient (m/s)
		φ_1:	Friction angle (deg)

(1) Equivalent harmonic, applied at the base of the liquefiable soil layer, (2) average value for the natural and the improved soil layers

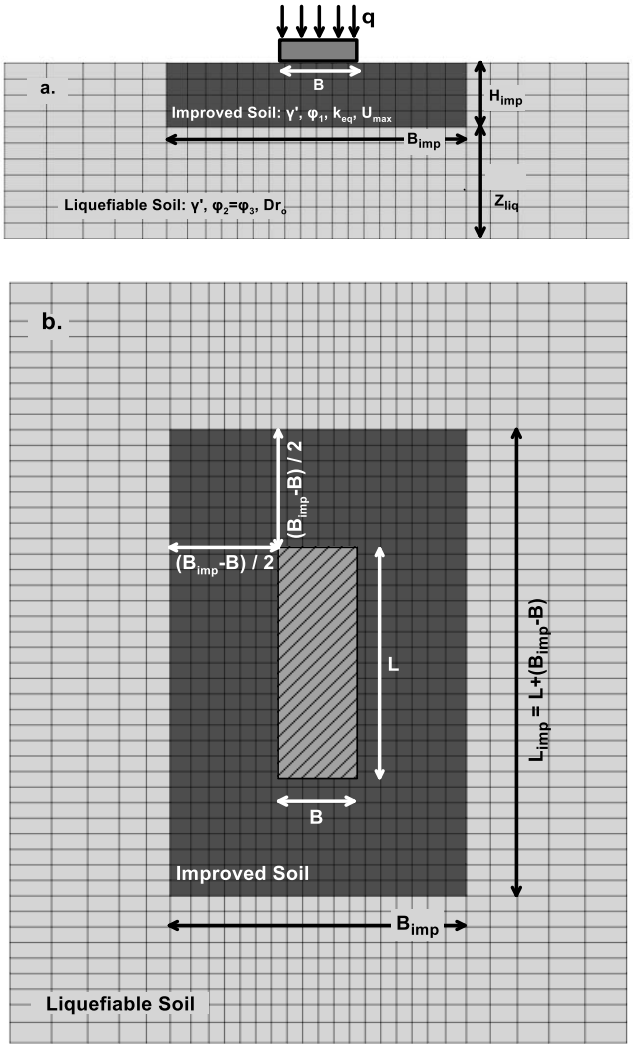

Figure A.1: (a) Cross section and (b) Plan view of the footing and the improved soil area.

Table A.2: Computation of degraded Bearing Capacity and associated Factor of Safety

$$FS_{\deg} = \frac{q_{ult,\deg}}{q}$$

$$q_{ult,\deg} = q_{ult,\deg}^{\inf} I_{q,size}$$

$$I_{q,size} = 1 - \exp\left[-C_{q,size} \left(\frac{H_{imp}}{B} \right)^{-1.90} \left(\frac{B_{imp}}{B} \right)^{0.15} \right]$$

$$C_{q,size} = 0.38\left(1 + 0.12\frac{L}{B}\right) \le 0.65$$

$$q_{ult,\deg}^{\inf} = \min\left\{ \begin{array}{r} \frac{1}{2}\gamma' \cdot B \cdot N_{\gamma 1,\deg} F_{\gamma s} \\ \gamma' \mathrm{H}_{imp}{}^{2} \mathrm{K}_{s} \frac{\tan\varphi_{1,\deg}}{B} s + \gamma'\left[(1+\alpha)^{2} - 1\right] \mathrm{H}_{imp}{}^{2} \mathrm{K}_{s} \frac{\tan\varphi_{2,\deg}}{B} s - \gamma'(1+\alpha) H_{imp} + \\ + \frac{1}{2}\gamma' \cdot B \cdot N_{\gamma 3,\deg} F_{\gamma s} + \gamma'(1+\alpha) H_{imp} N_{q3,\deg} F_{qs} \end{array} \right.$$

$$\alpha = 3.76\left[\frac{k_{eq} T_{exc} N}{H_{imp}} \right]^{0.256}$$

$$K_{s} = \left(\frac{q}{p_{\alpha}} \right)^{-0.40} \left(\frac{H_{imp}}{B} \right)^{-0.50}$$

$$N_{q3,\deg} = \tan^{2}\left(45 + \varphi_{3,\deg}/2\right) e^{\pi \tan\varphi_{3,\deg}}, \quad N_{\gamma 3,\deg} = 2\left(N_{q3,\deg} + 1\right)\tan\varphi_{3,\deg}$$

$$\varphi_{i,\deg} = \tan^{-1}\left[(1 - U_{i})\tan\varphi_{i}\right]$$

$$U_{1} = 0.54 U_{\max}$$

$$U_{2} = 0.5 + 0.27 U_{\max}$$

$$U_{3} = 1.42 N^{0.13} D_{r,o}{}^{-0.28} \left(\frac{\overline{H}_{\mathrm{imp}}}{B} \right)^{-0.25} \left(\frac{Z_{liq}}{B} \right)^{0.22} \left(\frac{T_{exc}}{T_{soil}} \right)^{0.25} F_{u} \le 0.9$$

$$\overline{H}_{imp} = \max\left(\mathrm{H}_{imp}, B\right)$$

$$F_{u} = 0.75 + 0.05\frac{L}{B} \le 1.0$$

$$F_{\gamma s} = 1 - 0.4\frac{B}{L}$$

$$F_{qs} = 1 + \frac{B}{L}\tan\varphi_{3,\deg}$$

$$s = 1 + \frac{B}{L}$$

Table A.3: Computation of seismic settlements ρ_{dyn}

$$\rho_{dyn} = \rho_{dyn}^{inf} \cdot I_{\rho,size}$$

$$I_{\rho,size} = 1 - \exp\left[-C_{\rho,size} \left(\frac{H_{imp}}{B} \right)^{-1.00} \left(\frac{B_{imp}}{B} \right)^{0.30} \right]$$

$$C_{\rho,size} = 0.48 \left(1 + 0.26 \frac{L}{B} \right) \leq 1.00$$

$$\rho_{dyn}^{inf} = 0.017 \alpha_{max} \left(T_{exc} + T_{soil} \right)^2 N \left(\frac{1}{FS_{deg}^{inf}} \right)^{0.50} \left[1 + 0.15 \left(\frac{1}{FS_{deg}^{inf}} \right)^5 \right]$$

$$T_{soil} = \frac{4 H_{imp}}{V_{s,imp}} + \frac{4 Z_{liq}}{V_{s,sand}}$$